



Mix design optimization of low-grade MgO-based magnesium phosphate cement mortars for cold weather applications

Yakov Ermolov ^a, Matvey Trutnev ^a, Sergey Tsvetkov ^a, Anton Kasprzhitskii ^a,
Georgy Lazorenko ^a *

^a: Climate Center, Novosibirsk State University , Novosibirsk 630090, Russia

* Corresponding author: glazorenko@yandex.ru

Abstract

The utilization of low-grade MgO in magnesium phosphate cement (MPC) systems offers significant economic and environmental benefits, yet its performance is often limited by reduced reactivity and sensitivity to curing conditions, particularly at low temperatures. In this study, magnesium ammonium phosphate cement (MAPC) and magnesium potassium phosphate cement (MKPC) mortars were systematically developed using low-grade MgO in combination with ammonium dihydrogen phosphate (ADP) or potassium dihydrogen phosphate (KDP). A sequential optimization strategy was applied to determine the optimal mix design, followed by hydration heat measurements and mechanical performance evaluation after curing under ambient ($25 \pm 2^\circ\text{C}$) and sub-zero conditions (up to -20°C). The results demonstrate that under ambient curing, MKPC achieved the highest compressive strength (30 MPa at 3 days), while MAPC reached 23 MPa. Sub-zero curing resulted in a reduction of approximately 30-36%. The peak hydration temperature decreased from 100°C to 79°C for MAPC and from 37°C to 12°C for MKPC under sub-zero conditions. Apparent porosity increased from 6-9% to higher values depending on curing conditions, indicating a less dense microstructure. Microstructural characterization of hardened specimens using scanning electron microscopy (SEM), X-ray diffraction (XRD) and Fourier-transform infrared spectroscopy (FTIR) revealed differences in the formation, morphology, and continuity of struvite-type hydration products, which govern the observed mechanical performance. The findings provide a practical framework for designing sustainable MPC mortars and highlight the potential of such systems for cold-weather construction applications.

Key findings

- Hydration heat measurements reveal reduced peak temperatures and slower reaction kinetics under sub-zero conditions.
- Low-temperature curing limits early strength development through reduced reaction rates in MPC mortars.
- Microstructural observations indicate less dense and less continuous binding phases under sub-zero curing conditions.

© 2026, the Authors. This article is published in open access under the terms and conditions of the Creative Commons Attribution (CC BY) license (<http://creativecommons.org/licenses/by/4.0/>), which permits unrestricted reuse of the work in any medium provided the original work is properly cited.

1. Introduction

Magnesium phosphate cements (MPC) are a class of rapid-setting inorganic binders that have attracted increasing attention due to their high early strength [1-3], low shrinkage [4,5], and excellent bonding to existing sub-

strates [6,7]. These characteristics make MPC particularly suitable for repair applications and for use under adverse environmental conditions, including low-temperature and cold-climate scenarios [9-11]. Among MPC systems, magnesium ammonium phosphate cement (MAPC) [12,13] and magnesium potassium phosphate cement (MKPC) [14,15]

Accompanying information

Article history

Received: 27.03.2026

Revised: 02.05.2026

Accepted: 02.05.2026

Available online: 02.05.2026

Keywords

Magnesium phosphate cement; low-grade MgO; sub-zero curing; hydration kinetics; mechanical properties.

Funding

This work was supported by the Russian Science Foundation (grant no. 24-79-10320, <https://rscf.ru/en/project/24-79-10320/>).

Supplementary information

Transparent peer review:

Sustainable Development Goals



are the most widely studied, with their performance governed by the formation of struvite-type hydration products and the kinetics of acid-base reactions between MgO and phosphate precursors.

Despite their promising properties, the large-scale application of MPC is constrained by the cost and availability of highly reactive MgO, which is typically produced under controlled calcination conditions [16-18]. In this context, the use of low-grade magnesia (LM), including by-products and dust fractions from industrial processes [19], represents an attractive alternative from both economic and sustainability perspectives. However, LM is generally characterized by lower reactivity and compositional variability, which can significantly affect hydration kinetics, heat evolution, and strength development [20-22]. These challenges are further exacerbated under sub-zero curing conditions, where reduced reaction rates and partial freezing of the pore solution may hinder the formation of binding phases.

Previous studies have demonstrated that the performance of MPC systems is highly sensitive to mix design parameters [23,24]. The MgO-to-phosphate (M/P) ratio is widely recognized as a governing parameter controlling hydration kinetics and phase formation. A moderate increase in the M/P ratio accelerates MgO dissolution and promotes rapid formation of struvite-type phases, leading to enhanced early strength [25,26]. However, both insufficient and excessive MgO contents are detrimental. Low M/P ratios result in incomplete phosphate reaction and increased porosity, whereas high ratios may cause excessive heat release, unreacted MgO, and structural instability. Quantitatively, the influence of M/P on compressive strength is particularly pronounced, with contribution rates exceeding 70-80% for early- and later-age strength development [27]. The water-to-cement (W/C) ratio also plays a critical role by regulating ion transport and pore structure evolution. At room temperature, compressive strength of MPC based on dead-burned magnesia (DBM) decreases markedly when W/C exceeds ~0.20, while very low values (<0.12) impair workability [28]. In addition to mix design, curing temperature is a critical factor controlling hydration and strength development. Unlike Portland cement, MPC systems are capable of setting and hardening even at -20 °C due to the exothermic nature of the acid-base reaction [29]. Nevertheless, decreasing temperature significantly alters hydration pathways. Reduced ion mobility and partial freezing lead to lower crystallinity of struvite phases and a pronounced drop in early strength. For example, the 28-day strength of MPC cured at -20 °C may decrease to approximately 65-80% of that achieved under ambient conditions [28]. This interplay highlights the need for systematic optimization strategies that simultaneously account for compositional parameters and environmental exposure. Nevertheless, most existing studies have considered either mix design optimization or temperature effects in isolation, and systematic investigations

combining both aspects for low-grade MgO-based MPC mortars remain limited. In addition, comparative analyses between MAPC and MKPC systems under identical conditions are relatively scarce, especially with regard to hydration heat evolution and microstructural development under sub-zero exposure. Recent studies have enhanced the understanding of hydration kinetics and microstructural evolution in MPC systems, particularly for MKPC-based materials [30-32]; however, these findings are largely derived from systems employing highly reactive MgO under controlled conditions.

In this study, MPC mortars based on low-grade MgO were developed using MAPC and MKPC systems. A sequential optimization strategy was adopted to identify optimal M/P and W/C ratios, followed by evaluation of hydration behavior and compressive strength under both laboratory and outdoor sub-zero curing conditions. Hydration heat evolution was monitored to assess reaction kinetics, while microstructural and phase analyses were performed to elucidate the mechanisms governing performance. The main objective of this work is to establish a link between mix design, curing conditions, and resulting properties of low-grade MgO-based MPC mortars. The findings contribute to the development of cost effective MPC systems and provide insight into their applicability in cold weather construction.

2. Experimental program

2.1. Raw materials

In this work, MgO source was provided by a low-grade magnesia (LM) powder. The material, supplied by Magnezit Group (Russia), consists of fine particulate matter (particle size < 90 µm) recovered during the production of sintered periclase. According to the supplier's specifications, the MgO content exceeds 86 wt.%, and the loss on ignition is approximately 6.8%, reflecting the presence of residual volatiles and partially unreacted phases. The material is characterized by a specific surface area of 19 m²/g, and its particle size distribution is shown in **Figure 1**. The reactivity of the MgO was evaluated using the citric acid activity (CAA) test, which is widely employed to assess the hydration reactivity of magnesia. The measured neutralization time was 820 ± 25 s, indicating relatively low reactivity in comparison with values typically reported for more reactive MgO [33,34]. Two phosphate precursors were employed to produce different MPC systems: potassium dihydrogen phosphate (KDP, KH₂PO₄, ≥99% purity) and ammonium dihydrogen phosphate (ADP, NH₄H₂PO₄, ≥99% purity), both provided by Ruskhim. Borax (Na₂B₄O₇·10H₂O, ≥99% purity), supplied by Eti Maden (Türkiye), was used as a setting retarder. Natural quartz sand with a particle size range of 0.1-2 mm was used as the fine aggregate. Deionized water at room temperature was employed for all mixtures.

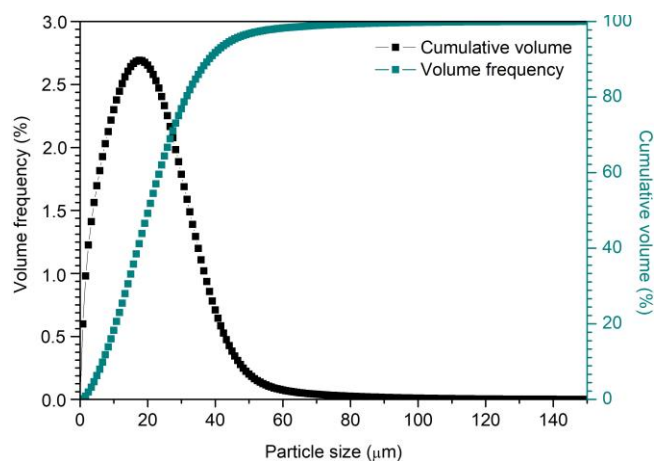


Figure 1 Particle size distribution of the low-grade MgO used in this study.

2.2. Mix proportions and specimen preparation

Magnesium phosphate cement mortars were prepared using LM in combination with ADP or KDP. All experiments were conducted using a single source of LM with fixed borax dosage (10 wt.% of MgO) and a constant sand-to-cement mass ratio of 1:1. The sand content and borax dosage were kept constant for all mixtures, while the MgO-to-phosphate (M/P) mass ratio and water-to-cement (W/C) mass ratio were varied (**Figure 2**). A two-stage optimization approach was adopted, involving systematic variation of the M/P ratio followed by adjustment of the W/C ratio to identify optimal formulations for both MAPC and MKPC systems. The selection of M/P and W/C ratios as primary variables was motivated by their dominant influence on hydration kinetics and strength development in MPC systems [35,36]. Other parameters (such as retarder dosage and particle size distribution of MgO) were intentionally kept constant to reduce experimental complexity and isolate the main compositional effects, particularly under variable temperature conditions.

It should be noted that the roles of MgO reactivity, water content, and borax addition are associated with different aspects of the MPC reaction process. The relatively low reactivity of the LM primarily limits the rate of Mg^{2+} release into solution, which justifies the use of a higher W/C ratio to facilitate ion transport and interaction between reactants [33,34]. In contrast, borax mainly affects the subsequent formation of hydration products by delaying the nucleation and growth of struvite-type phases through Mg^{2+} complexation and modification of solution chemistry [37,38]. In this context, the fixed borax dosage and adjusted W/C ratio can be considered as complementary measures enabling controlled reaction kinetics and consistent workability across the investigated compositions.

Following the two-stage optimization of MAPC and MKPC mixtures conducted under laboratory conditions (25 ± 2 °C, $RH = 36 \pm 4\%$), a subsequent experimental stage was designed to evaluate the influence of outdoor sub-zero curing on hydration behavior and early-age compressive strength. For this purpose, all solid components (LM, ADP,

KDP, borax, and sand), as well as the steel molds, were pre-conditioned under outdoor winter conditions for 1 h prior to mixing to establish a consistent initial temperature state representative of field exposure. Distilled water was maintained at 22 ± 2 °C, and mixing was carried out in an outdoor sub-zero conditions. This water temperature was chosen to simulate practical mixing conditions (water often stored indoors) and to ensure sufficient initial reaction activation, allowing systematic comparison between laboratory and outdoor curing without introducing water temperature as an additional variable. The potential for colder water in some extreme field scenarios is acknowledged as a limitation of the study. The temporal variation of temperature and relative humidity during the curing period is presented in **Figure 3**. Mixing was carried out by first homogenizing the dry constituents, followed by the addition of water and further mixing for 30 s to obtain a uniform paste. The fresh mixtures were then cast into steel cube molds with dimensions of $20 \times 20 \times 20$ mm³. Before casting, the inner surfaces of the molds were coated with a wax-silicone release agent applied in two layers to reduce adhesion and facilitate specimen removal. For comparison, control series of specimens were prepared and cured entirely under laboratory conditions.

2.3. Test methods

Uniaxial compressive strength (UCS) was measured on cubic specimens using a universal testing machine (REM-20-A-0.5-1, Metrotest, Russia) under displacement-controlled loading at a rate of 3 mm/min. Specimens were tested after 3 days of curing. For each mix composition, a minimum of ten specimens were prepared, and the reported values represent the average of valid measurements. Specimens exhibiting visible casting defects or anomalous responses were excluded prior to analysis. The temperature evolution during hydration was monitored by embedding a temperature probe at the center of a 50 mm cubic specimen. Temperature data were recorded continuously with a resolution of 0.1 °C and an instrumental accuracy of ± 0.2 °C. Bulk density and voids content were determined in accordance with ASTM C642-21. A DA-1203C balance (BEL Engineering, Italy) was employed for weighing, with a maximum load of 1200 g and a resolution of 0.01 g. Phase assemblage was examined by X-ray diffraction using a DRON-8 diffractometer (Burevestnik, Russia) with Cu $K\alpha$ radiation ($\lambda = 1.5406$ Å). Data acquisition was carried out over a 2θ interval of $2-65^\circ$, employing an angular increment of 0.05° and a dwell time of 3 s per step. Infrared characterization was performed with an FT-805 spectrometer (NPF SIMEX, Russia) using the KBr pellet technique. Spectra were collected in the range of $500-4000$ cm⁻¹ at a resolution of 4 cm⁻¹, with each spectrum obtained by averaging a minimum of 50 scans. Microstructural features of fracture surfaces were analyzed by scanning electron microscopy (Hitachi S3400N) operated at an accelerating voltage of 20 kV in backscattered electron mode.

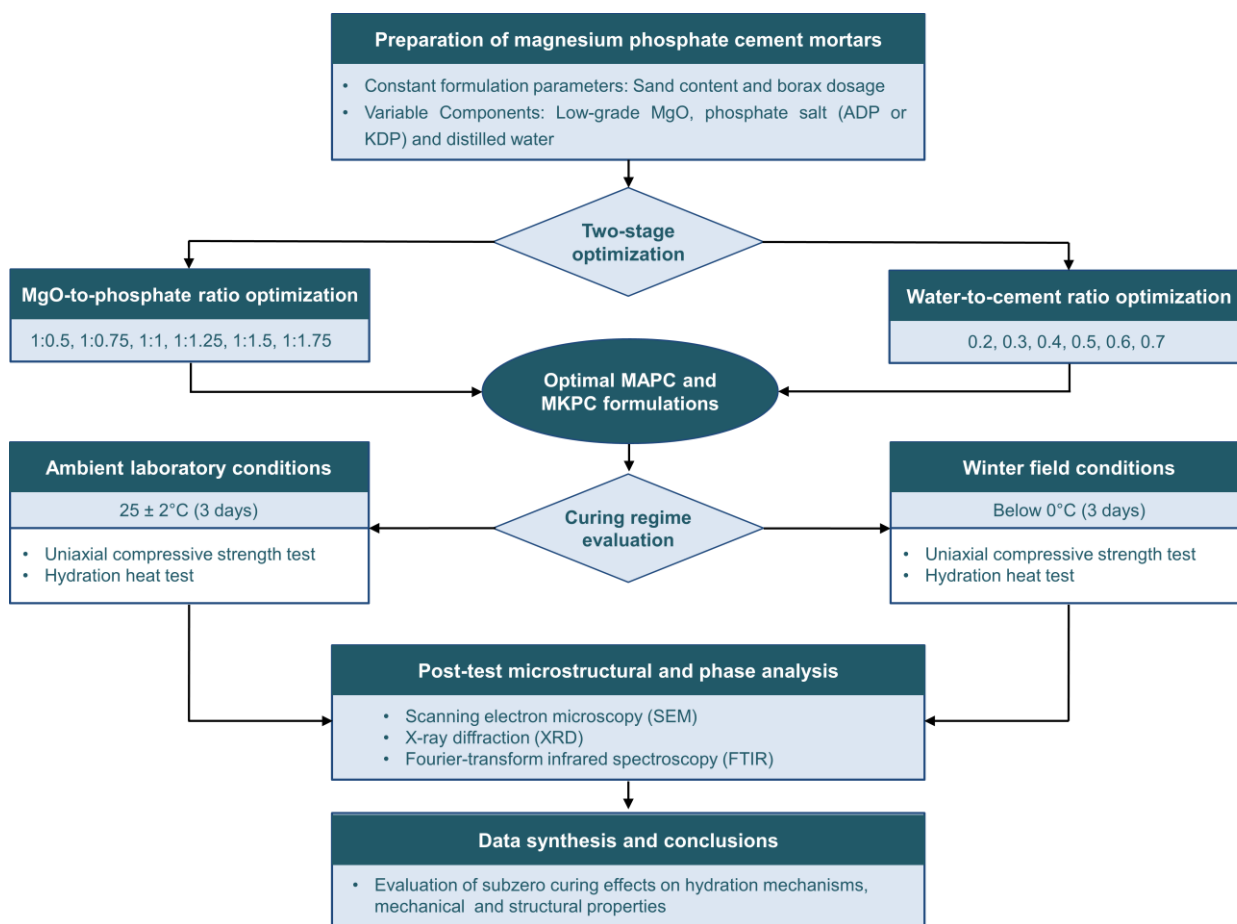


Figure 2 Experimental design flowchart for the development and characterization of magnesium phosphate cement mortars based on low-grade MgO with ADP and KDP.

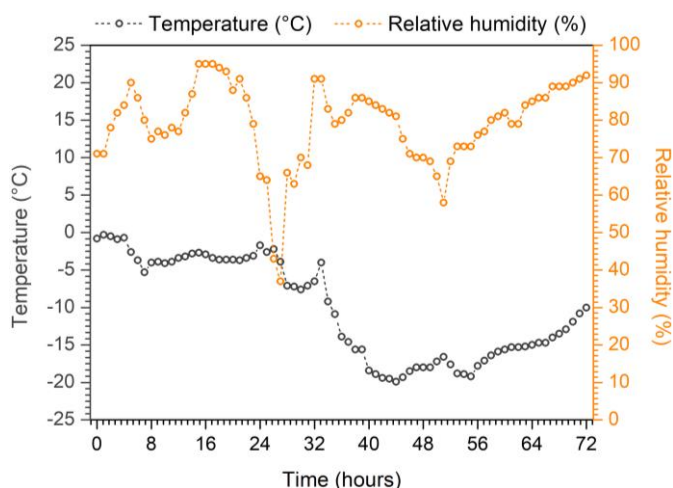


Figure 3 Variation of temperature and relative humidity over 72 h under outdoor sub-zero conditions during mortar curing.

3. Results and discussion

3.1. Effects of M/P and W/C ratios

The influence of the MgO-to-phosphate ratio on compressive strength is presented in **Fig. 4a**. During the M/P ratio optimization stage, the W/C ratio was fixed at 0.5. For both MAPC and MKPC mortars, a pronounced increase in strength is observed with increasing M/P ratio up to an optimum, followed by a decline at higher values. In the case of MAPC, compressive strength increases sharply

from ~2 MPa at M/P = 1:0.5 to a maximum of ~19 MPa at M/P = 1:1.25, after which it decreases to ~14 MPa at M/P = 1:1.75. A similar trend is observed for MKPC, although with consistently higher strength values, reaching a maximum of ~24 MPa at M/P = 1:1.25. This behavior can be attributed to the balance between MgO availability and phosphate supply governing the formation of struvite-type phases [39]. At low M/P ratios, insufficient MgO limits the extent of the acid-base reaction, resulting in incomplete phase formation and low strength. Increasing the M/P ratio enhances MgO dissolution and promotes rapid nucleation and growth of hydration products, leading to a denser microstructure [40]. However, excessive MgO at high M/P ratios leads to the presence of unreacted particles and increased heterogeneity, which adversely affects mechanical performance [41,42].

The effect of the water-to-cement ratio on compressive strength is shown in **Fig. 4b**. Both systems exhibit a well-defined optimum at intermediate W/C values, with maximum strength achieved at W/C = 0.4. At lower W/C ratios, insufficient water restricts ion mobility and limits the extent of reaction, resulting in reduced strength (~3 MPa for MAPC and ~12 MPa for MKPC). Increasing W/C to 0.4 significantly enhances strength, reaching ~23 MPa for MAPC and ~30 MPa for MKPC. Further increases in W/C ratio lead to a progressive decline in strength, with values dropping to below ~10 MPa for MAPC at W/C ≥ 0.6.

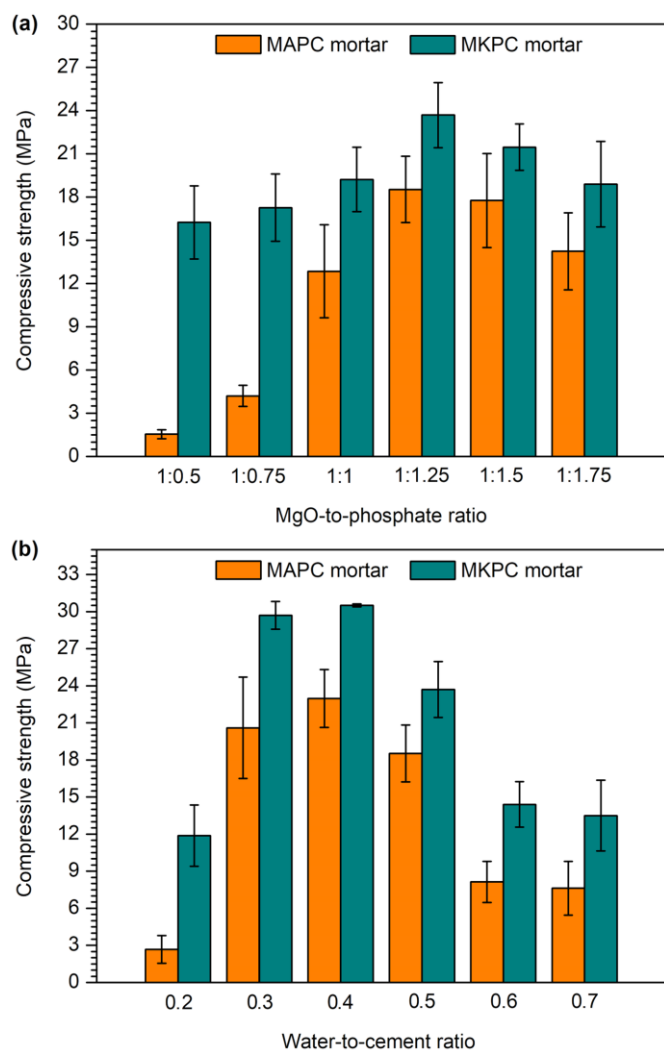


Figure 4 Effect of (a) MgO-to-phosphate (M/P) ratio and (b) water-to-cement (W/C) ratio on the compressive strength of MAPC and MKPC mortars.

The observed trends reflect the dual role of water in MPC systems. Adequate water content is required to ensure effective dissolution of reactants and transport of ionic species, facilitating the formation of a continuous binding matrix [43]. However, excessive water increases porosity and weakens the hardened structure [44]. It should be noted that the optimal W/C ratio of 0.4 observed in this study is slightly higher than the values commonly reported for MPC systems based on highly reactive MgO (0.2-0.3 [45,46]), which may be associated with differences in MgO reactivity. Notably, MKPC consistently exhibits higher strength than MAPC across all compositions, which can be attributed to differences in reaction kinetics and the stability of potassium-based struvite phases [47-49]. This trend is consistent with recent findings reported by Li et al. [48].

From the perspective of mixture design, both M/P and W/C ratios critically control the mechanical performance of MPC mortars, with optimal compositions identified at M/P = 1:1.25 and W/C = 0.4 for both MAPC and MKPC systems. These optimized mixtures were selected for subsequent investigation under different curing conditions.

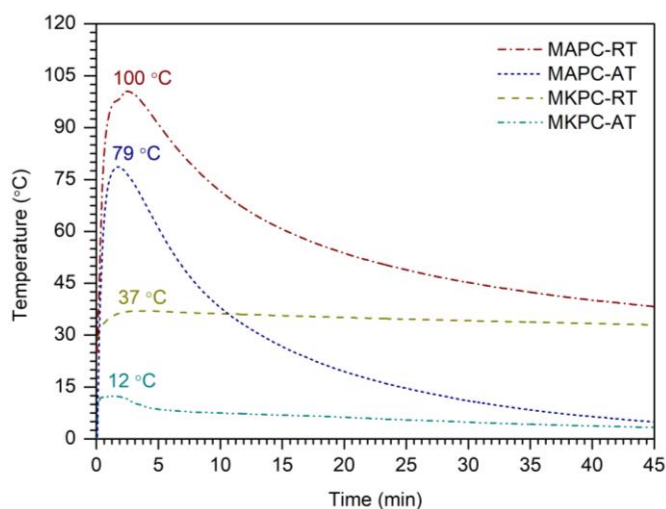


Figure 5 Temperature evolution during hydration of MAPC and MKPC mortars under outdoor winter (AT) and room-temperature (RT) conditions.

3.2. Curing effects on strength and hydration heat

The temperature evolution during hydration under room-temperature (RT) and outdoor sub-zero (AT) conditions is presented in **Figure 5**.

Under RT conditions, both MAPC and MKPC systems exhibit rapid and highly exothermic reactions, with peak temperatures reaching 100 °C and 37 °C, respectively. In contrast, curing under AT conditions significantly suppresses the exothermic response, reducing peak temperatures to 79 °C for MAPC and 12 °C for MKPC, and leading to a faster decay of the temperature profiles (**Figure 5**). The observed reduction in peak temperature and heat release under sub-zero conditions indicates a substantial slowdown in reaction kinetics due to decreased ion mobility and partial freezing of the pore solution. This effect is particularly pronounced for MKPC, where the already moderate exothermicity is further diminished, resulting in a low thermal activation of the system. These changes in hydration heat evolution directly affect early-age strength development. Lower peak temperatures and reduced heat release under AT conditions limit the extent and rate of struvite formation, leading to delayed hardening and reduced early compressive strength compared to RT curing. In contrast, the higher heat evolution under RT conditions promotes rapid phase formation and densification of the microstructure, resulting in enhanced mechanical performance at early ages. This behavior is consistent with the findings of Yuan et al. [50,51], who demonstrated that decreasing curing temperature markedly retards MPC hydration kinetics and strength development due to reduced dissolution rates and hindered crystallization processes. The results presented in **Fig. 6** reveal a interrelation between compressive strength, bulk density, and apparent porosity for both MAPC and MKPC mortars under different curing regimes. Under room-temperature conditions, MKPC exhibits the highest compressive strength (~30 MPa), accompanied by the highest bulk density

($\sim 2.0 \text{ g/cm}^3$) and the lowest apparent porosity ($\sim 6\text{--}9\%$). In contrast, MAPC mortars show lower strength ($\sim 23 \text{ MPa}$), reduced density ($\sim 1.5 \text{ g/cm}^3$), and significantly higher porosity ($\sim 18\text{--}19\%$), indicating a comparatively less compact microstructure.

Under outdoor sub-zero curing conditions, both MAPC and MKPC mortars exhibit a reduction in compressive strength, amounting to approximately 36% and 30%, respectively. These changes are accompanied by an increase in apparent porosity, which is particularly evident for the MKPC system, indicating modifications in the internal structure of the materials formed under low-temperature conditions. The increase in apparent porosity under sub-zero curing can be attributed to the suppression of hydration kinetics and incomplete formation of binding phases, as well as the potential formation of ice within the pore structure, which disrupts matrix continuity [52,53]. This effect is more evident in MAPC, where the increase in porosity is accompanied by a corresponding reduction in strength, suggesting a greater sensitivity of the system to sub-zero curing conditions. In contrast, MKPC retains a comparatively higher density and lower porosity under similar conditions, indicating a more compact structure, although it is still affected by low-temperature curing. **Table 1** summarizes representative compressive strength data reported for MPC systems in recent studies, in comparison with the results of the present work. The data illustrate the variability in strength development depending on MgO reactivity, mix design, and curing conditions, and provide a basis for contextualizing the performance of the proposed formulations.

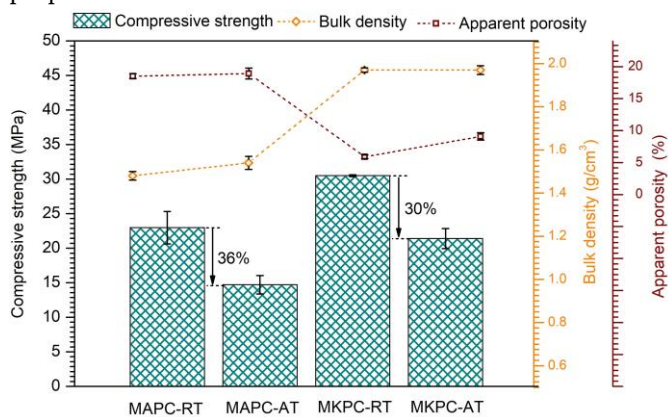


Figure 6 Compressive strength, bulk density, and apparent porosity of MAPC and MKPC mortars cured under room-temperature (RT) and outdoor sub-zero (AT) conditions.

Table 1 Comparison of mechanical performance of MPC systems reported in recent studies and in the present work.

Study	System	MgO type	Curing conditions	3-day UCS (MPa)
This work	MAPC	LM	0...-20°C	14.7
This work	MKPC	LM	0...-20°C	21.4
Luo et al. [54]	MKPC	DBM ^a	-5°C	20
Wang et al. [55]	MAPC	LBM ^b	-20°C	21.7

^a Dead burnt magnesia;

^b Light burnt magnesia.

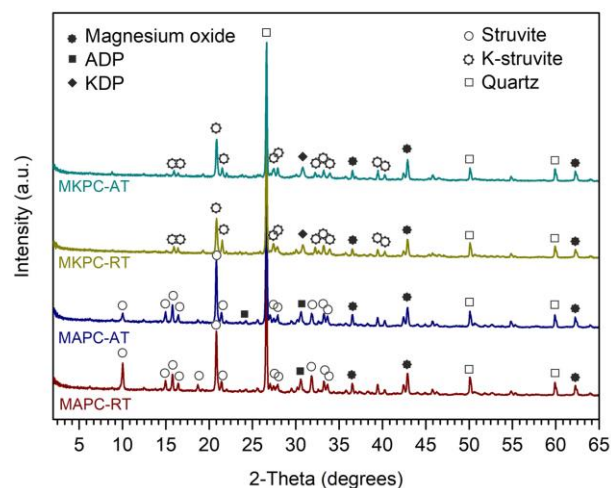


Figure 7 XRD patterns of MAPC and MKPC mortars cured under outdoor winter (AT) and room-temperature (RT) conditions.

3.3. Microstructural and phase characterization

The XRD patterns (**Figure 7**) confirm that the dominant crystalline products formed in both MAPC and MKPC systems correspond to struvite-type phases. In the MAPC samples, reflections associated with struvite ($\text{MgNH}_4\text{PO}_4 \cdot 6\text{H}_2\text{O}$) are clearly observed, while in the MKPC system the formation of K-struvite ($\text{MgKPO}_4 \cdot 6\text{H}_2\text{O}$) is evident. Residual peaks of unreacted MgO and phosphate precursors (ADP or KDP) are still detectable, indicating incomplete reaction of the starting materials, particularly under sub-zero curing conditions. The reflections attributed to quartz from the aggregate phase are consistently present in all samples and do not vary with curing conditions. Comparison between RT and AT conditions suggests a slight reduction in the relative intensity and sharpness of struvite-type reflections in the samples cured under outdoor sub-zero conditions, which may be associated with a lower degree of crystallinity and/or less complete development of hydration products at low temperatures. Owing to the qualitative nature of the XRD analysis, the observed differences do not allow a definitive assessment of changes in crystallinity.

At the same time, the persistence of precursor-related peaks under AT conditions indicates that reduced reaction kinetics limit the extent of MgO dissolution and subsequent precipitation of phosphate hydrates.

The FTIR spectra (**Fig. 8**) further support these observations. All samples exhibit characteristic bands associated with phosphate groups (ν_1 and ν_3 PO_4 vibrations in the range $900\text{--}1100 \text{ cm}^{-1}$) [56,57], which partially overlap with Si-O-Si stretching vibrations originating from the quartz fraction [58-60]. Additional bands corresponding to structural water are observed as H-O-H bending ($\sim 1650 \text{ cm}^{-1}$) and broad stretching vibrations in the range $3000\text{--}3500 \text{ cm}^{-1}$ [61-63]. In MAPC samples, the band near 1430 cm^{-1} is attributed to $\delta(\text{NH}_4^+)$, confirming the presence of ammonium-containing hydration products [64]. The presence of these bands confirms the formation of hydrated phosphate phases consistent with XRD results.

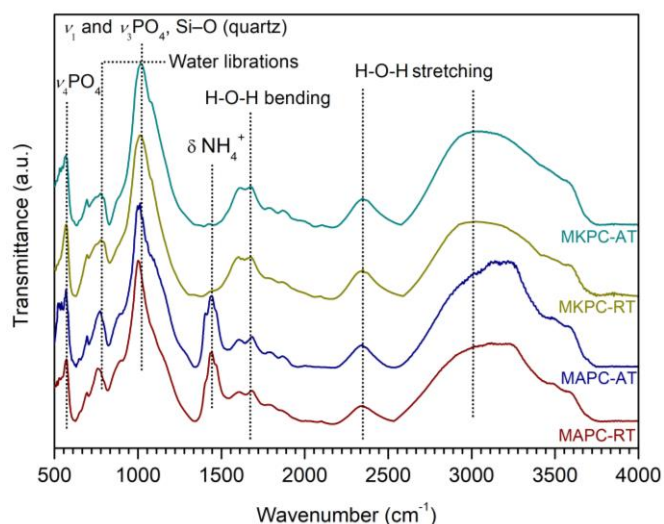


Figure 8 FTIR spectra of MAPC and MKPC mortars cured under outdoor winter (AT) and room-temperature (RT) conditions.

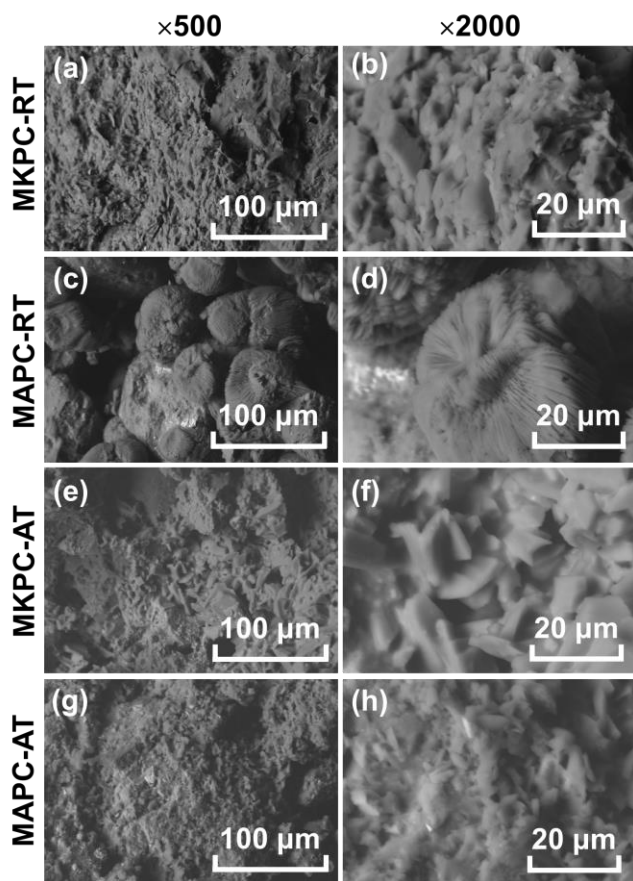


Figure 9 SEM micrographs of MKPC and MAPC mortars cured under room-temperature (RT) and outdoor sub-zero (AT) conditions at $\times 500$ and $\times 2000$ magnifications.

Under sub-zero curing conditions, a slight broadening and reduction in intensity of phosphate-related bands can be observed, indicating a less ordered structure and a lower degree of hydration [57,65,66].

The SEM micrographs (**Figure 9**) further elucidate the influence of curing conditions on the microstructural development of MAPC and MKPC mortars. Under RT conditions, MKPC exhibits a relatively dense and continuous

matrix (**Figure 9a,b**), characterized by intergrown crystalline phases forming a compact structure. In contrast, MAPC (**Figure 9c,d**) shows well-defined prismatic and rosette-like struvite crystals, indicating a more heterogeneous microstructure with distinct crystal boundaries. Exposure to sub-zero curing conditions leads to noticeable changes in morphology for both systems. In MKPC (**Figure 9e,f**), the structure becomes less compact, with a more fragmented arrangement of crystals and increased interparticle spacing. Similarly, MAPC (**Figure 9g,h**) exhibits a less developed and more loosely packed microstructure, where the crystalline features appear finer and less well-defined compared to RT conditions. The observed differences in crystal morphology may be related to changes in growth kinetics under sub-zero conditions and do not necessarily reflect variations in the overall degree of crystallinity. These observations are consistent with the XRD and FTIR results, indicating that sub-zero curing conditions suppress crystal growth and limit the development of well-ordered hydration products. The resulting microstructural coarsening and reduced packing density provide an explanation for the observed increase in porosity and corresponding decrease in compressive strength.

3.4. Discussion of MAPC and MKPC behavior

The behavior of MAPC and MKPC systems can be interpreted based on phosphate chemistry, crystallization characteristics, and temperature-dependent kinetics. Ammonium-based systems generally exhibit faster reaction rates and higher heat evolution, which is attributed to more rapid acid-base interactions and earlier attainment of supersaturation [48,49]. This explains the higher peak temperatures observed for MAPC in the present study. In contrast, MKPC systems tend to undergo more gradual crystallization, leading to the formation of a denser and more continuous microstructure, which is consistent with previous reports for MKPC-based systems [14,15] and with the observations of this work.

Under sub-zero curing conditions, both systems are affected by reduced ion mobility and partial freezing of the pore solution, which suppress hydration kinetics and limit the development of crystalline phases [10,50,51]. However, MAPC retains relatively higher heat evolution, which may partially compensate for low ambient temperatures, whereas MKPC exhibits significantly reduced heat release, resulting in lower thermal activation. These combined effects explain the observed differences in reaction rate, heat evolution, and strength between the two systems.

From an application perspective, the observed differences between the two systems may also suggest a degree of complementarity under cold-weather conditions. While MKPC exhibits a relatively stable structural response, MAPC is characterized by higher heat evolution during hydration, which may contribute to partial internal thermal activation at low ambient temperatures. However,

this interpretation remains tentative and requires dedicated experimental validation.

4. Limitations

This study focuses on early-age performance, with curing limited to 3 days, and therefore does not address long-term strength development or durability. The experimental program was conducted using a single low-grade MgO source and fixed sand and borax contents, which may limit the generality of the findings. In addition, outdoor sub-zero curing was performed under monitored field conditions, which enhances practical relevance but limits environmental controllability, particularly with respect to temperature fluctuations and humidity. Furthermore, the sequential optimization approach adopted in this study does not fully capture potential interaction effects between M/P ratio, W/C ratio, and curing temperature. While this approach enables clear identification of primary trends, a more comprehensive multivariable design would be required to systematically evaluate coupled effects. In addition, pore structure characterization was limited to apparent porosity measurements, and more advanced techniques such as mercury intrusion porosimetry (MIP) or X-ray computed tomography (CT) would provide deeper insight. Future studies will address these aspects, including long-term performance, multivariable optimization, and controlled curing conditions.

5. Conclusions

This study demonstrates that the performance of low-grade MgO-based magnesium phosphate cement mortars is governed by both mix design parameters and curing temperature. A sequential optimization strategy enabled the identification of optimal MgO-to-phosphate and water-to-cement ratios for MAPC and MKPC mortars, providing a consistent basis for systematically assessing their behavior under low-temperature conditions.

The results show that curing under outdoor sub-zero conditions (down to $-20\text{ }^{\circ}\text{C}$) affects the development of the internal structure, leading to reduced compressive strength, increased apparent porosity, and slight changes in bulk density. These effects are attributed to the suppression of hydration kinetics and limitations in crystal growth at low temperatures. Despite these changes, XRD and FTIR analyses confirm that the fundamental hydration products remain unchanged, with struvite-type phases forming in both systems regardless of curing regime.

Microstructural observations further indicate that low-temperature curing leads to less developed and more heterogeneous structures, characterized by reduced intergrowth of crystalline phases and less efficient packing. These features are consistent with the observed macroscopic performance and reflect the influence of temperature on early-stage hydration processes.

In summary, the results provide a systematic evaluation of the effect of sub-zero curing on MPC systems and enable an assessment of their performance potential under cold-climate conditions. While MKPC exhibits a more stable structural response at low temperatures, MAPC is characterized by a significantly higher heat evolution during hydration, which may be advantageous for mitigating the effects of low ambient temperatures. In this context, the observed differences between MAPC and MKPC suggest potential complementarity in their performance under cold-weather conditions. However, this hypothesis requires dedicated experimental validation, which warrants further investigation.

Supplementary materials

No supplementary materials are available.

Data availability statement

Data will be made available on request.

Acknowledgments

None.

Author contributions

Conceptualization: G.L.
Data curation: Y.E.
Formal Analysis: G.L, A.K.
Investigation: Y.E., M.T., S.T.
Methodology: G.L, Y.E.
Project administration: G.L.
Validation: G.L., A.K.
Visualization: Y.E.
Writing – original draft: G.L, A.K.

Conflict of interest

The authors declare no conflict of interest.

Additional information

Author Scopus IDs:

Yakov Ermolov, [56872949600](https://orcid.org/56872949600);
Sergey Tsvetkov, [60058194000](https://orcid.org/60058194000);
Anton Kasprzhitskii, [16042848600](https://orcid.org/16042848600);
Georgy Lazorenko, [56070005300](https://orcid.org/56070005300).

Website:

Climate Center, Novosibirsk State University,
<https://www.nsu.ru/n/research/climatic-center/>.

References

1. He ZH, Jiang YY, Shi JY, Qin J, Liu DE, Yalçinkaya Ç, He YF. Effect of silica fume on the performance of high-early-strength UHPC prepared with magnesium ammonium phosphate cement. *Case Stud. Constr. Mater.* 2024; 20: e03351. [doi:10.1016/j.cscm.2024.e03351](https://doi.org/10.1016/j.cscm.2024.e03351)
2. You C, Qian J, Qin J, Wang H, Wang Q, Ye Z. Effect of early hydration temperature on hydration product and strength development of magnesium phosphate cement (MPC). *Cem. Concr. Res.* 2015; 78(5001): 179 – 189. [doi:10.1016/j.cemconres.2015.07.005](https://doi.org/10.1016/j.cemconres.2015.07.005)
3. Zhang J, Hu X, Shao W, Mook Lim Y, Chen Z, Zhu W. Experimental Study on Properties of Magnesium Phosphate Cement-Based Self-Compacting Concrete with High-Early Strength. *J.*

- Mater. Civ. Eng. 2022; 34(2): 04021435. [doi:10.1061/\(ASCE\)MT.1943-5533.0004075](https://doi.org/10.1061/(ASCE)MT.1943-5533.0004075)
4. Dong D, Huang Y, Pei Y, Zhang X, Cui N, Zhao P, Hou P, Lu L. Effect of spherical silica fume and fly ash on the rheological property, fluidity, setting time, compressive strength, water resistance and drying shrinkage of magnesium ammonium phosphate cement. *J. Build. Eng.* 2023; 63: 105484. [doi:10.1016/j.jobe.2022.105484](https://doi.org/10.1016/j.jobe.2022.105484)
 5. Pei H, Zhang S, Bai L, Hou D, Yang Q, Borana L. Early-age shrinkage strain measurements of the graphene oxide modified magnesium potassium phosphate cement. *Meas.: J. Int. Meas. Confed.* 2019; 139: 293 - 300. [doi:10.1016/j.measurement.2019.03.002](https://doi.org/10.1016/j.measurement.2019.03.002)
 6. Lu Z, Hu C, Lin T, Dai M. Interface bonding mechanism and strength evolution of magnesium potassium phosphate recycled concrete under long-term seawater immersion. *Constr. Build. Mater.* 2025; 505: 144748. [doi:10.1016/j.conbuildmat.2025.144748](https://doi.org/10.1016/j.conbuildmat.2025.144748)
 7. Jia L, Jia W, Guo J, Sun Y. Nano-silica-enhanced high-performance magnesium phosphate cement repair mortars: Optimization of interfacial bonding. *Constr. Build. Mater.* 2025; 490: 142447. [doi:10.1016/j.conbuildmat.2025.142447](https://doi.org/10.1016/j.conbuildmat.2025.142447)
 8. Kasprzhitskii A, Shevchenko R, Kruglikov A, Lazorenko G. Electronic structure and elastic properties of struvite-type hydrates $MgMPO_4 \cdot nH_2O$ ($M = NH_4, K, Na$): Implications for magnesium phosphate cement performance. *Comput. Condens. Matter.* 2026; 47: e01290. [doi:10.1016/j.cocom.2026.e01290](https://doi.org/10.1016/j.cocom.2026.e01290)
 9. Sun W, Qian W, Cao X, Ma Y, Wang D, Fan J, Chen T. Effect of sucrose on the mechanical properties of magnesium and potassium phosphate cements at low temperatures and its mechanism of action. *Case Stud. Constr. Mater.* 2024; 20: e02655. [doi:10.1016/j.cscm.2023.e02655](https://doi.org/10.1016/j.cscm.2023.e02655)
 10. Feng H, Shaikat AJ, Rin D, Zhang P, Gao D, Sheikh MN. Mechanical properties of high-ductility magnesium phosphate cement composite cured at low temperatures. *J. Build. Eng.* 2021; 44: 103275. [doi:10.1016/j.jobe.2021.103275](https://doi.org/10.1016/j.jobe.2021.103275)
 11. Feng H, Nie S, Guo A, Shen S, Gao D, Chen G. Flexural behavior of high ductility MPC-based composites under low-temperature curing. *Constr. Build. Mater.* 2021. 300: 124231. [doi:10.1016/j.conbuildmat.2021.124231](https://doi.org/10.1016/j.conbuildmat.2021.124231)
 12. Han W, Chen H, Li X, Zhang T. Thermodynamic modeling of magnesium ammonium phosphate cement and stability of its hydration products. *Cem. Concr. Res.* 2020; 138: 106223. [doi:10.1016/j.cemconres.2020.106223](https://doi.org/10.1016/j.cemconres.2020.106223)
 13. Gan X, Zhu Y, Ma K, Li L, Lu L. Water resistance, mechanical properties, hydration characteristic and microstructure of magnesium ammonium phosphate cement modified by polyvinyl alcohol powder. *Constr. Build. Mater.* 2024; 440: 137439. [doi:10.1016/j.conbuildmat.2024.137439](https://doi.org/10.1016/j.conbuildmat.2024.137439)
 14. Gardner LJ, Bernal SA, Walling SA, Corkhill CL, Provis JL, Hyatt NC. Characterisation of magnesium potassium phosphate cements blended with fly ash and ground granulated blast furnace slag. *Cem. Concr. Res.* 2015; 74: 78 - 87. [doi:10.1016/j.cemconres.2015.01.015](https://doi.org/10.1016/j.cemconres.2015.01.015)
 15. Mo L, Lv L, Deng M, Qian J. Influence of fly ash and metakaolin on the microstructure and compressive strength of magnesium potassium phosphate cement paste. *Cem. Concr. Res.* 2018; 111: 116 - 129. [doi:10.1016/j.cemconres.2018.06.003](https://doi.org/10.1016/j.cemconres.2018.06.003)
 16. Chen Z, Lai Z, Zhang Y, Liu Z, Lu Z, Li J. Significance of low-temperature calcination in magnesite decomposition and its application in magnesium phosphate cement: A comprehensive study. *Ceram. Int.* 2025; 51 (11): 14619 - 14631. [doi:10.1016/j.ceramint.2025.01.300](https://doi.org/10.1016/j.ceramint.2025.01.300)
 17. Bouaoun I, Hammi H, Ait-Mokhtar A, El Amine Hamami A, M'Nif A. Effect of calcination temperature of magnesium silicate on the properties of magnesium phosphate cement. *J. Australas. Ceram. Soc.* 2017; 53 (2): 351 - 359. [doi:10.1007/s41779-017-0044-8](https://doi.org/10.1007/s41779-017-0044-8)
 18. Ribeiro DV, Paula GR, Morelli MR. Use of microwave oven in the calcination of MgO and effect on the properties of magnesium phosphate cement. *Constr. Build. Mater.* 2019; 198: 619 - 628. [doi:10.1016/j.conbuildmat.2018.11.289](https://doi.org/10.1016/j.conbuildmat.2018.11.289)
 19. Lazorenko G, Kasprzhitskii A. A review of magnesium-rich wastes and by-products as precursors for magnesium phosphate cements: Challenges and opportunities. *Environ. Res.* 2025; 285: 122402. [doi:10.1016/j.envres.2025.122402](https://doi.org/10.1016/j.envres.2025.122402)
 20. Niubó M, Formosa J, Maldonado-Alameda A, del Valle-Zermeño R, Chimenos JM. Magnesium phosphate cement formulated with low grade magnesium oxide with controlled porosity and low thermal conductivity as a function of admixture. *Ceram. Int.* 2016; 42 (13): 15049 - 15056. [doi:10.1016/j.ceramint.2016.06.159](https://doi.org/10.1016/j.ceramint.2016.06.159)
 21. Maldonado-Alameda A, Lacasta AM, Giro-Paloma J, Chimenos JM, Haurie L, Formosa J. Magnesium phosphate cements formulated with low grade magnesium oxide incorporating phase change materials for thermal energy storage. *Constr. Build. Mater.* 2017; 155: 209 - 216. [doi:10.1016/j.conbuildmat.2017.07.227](https://doi.org/10.1016/j.conbuildmat.2017.07.227)
 22. Formosa J, Lacasta AM, Navarro A, Del Valle-Zermeño R, Niubó M, Rosell JR, Chimenos JM. Magnesium Phosphate Cements formulated with a low-grade MgO by-product: Physico-mechanical and durability aspects. *Constr. Build. Mater.* 2015; 91: 150 - 157. [doi:10.1016/j.conbuildmat.2015.05.071](https://doi.org/10.1016/j.conbuildmat.2015.05.071)
 23. Fang B, Hu Z, Shi T, Liu Y, Wang X, Yang D, Zhu K, Zhao X, Zhao Z. Research progress on the properties and applications of magnesium phosphate cement. *Ceram. Int.* 2023; 49 (3): 4001 - 4016. [doi:10.1016/j.ceramint.2022.11.078](https://doi.org/10.1016/j.ceramint.2022.11.078)
 24. Yang N, Shi C, Yang J, Chang Y. Research progresses in magnesium phosphate cement-based materials. *J. Mater. Civ. Eng.* 2014; 26 (10): 04014071. [doi:10.1061/\(ASCE\)MT.1943-5533.0000971](https://doi.org/10.1061/(ASCE)MT.1943-5533.0000971)
 25. Haque MA, Chen B. Research progresses on magnesium phosphate cement: A review. *Constr. Build. Mater.* 2019; 211: 885 - 898. [doi:10.1016/j.conbuildmat.2019.03.304](https://doi.org/10.1016/j.conbuildmat.2019.03.304)
 26. Zheng Y, Zhou Y, Huang X, Luo H. Effect of raw materials and proportion on mechanical properties of magnesium phosphate cement. *J. Road Eng.* 2022; 2 (3): 243 - 251. [doi:10.1016/j.jreng.2022.06.001](https://doi.org/10.1016/j.jreng.2022.06.001)
 27. Zhang J, Li T, Yao Y, Hu X, Zuo Y, Du H, Yang J. Optimization of mix proportion and strength prediction of magnesium phosphate cement-based composites based on machine learning. *Constr. Build. Mater.* 2024; 411: 134738. [doi:10.1016/j.conbuildmat.2023.134738](https://doi.org/10.1016/j.conbuildmat.2023.134738)
 28. Jia XW, Luo JY, Zhang WX, Tang MH, Qian JS, Wang P, Li JM. Reaction characteristics and compressive strength of magnesium phosphate cement at negative temperatures. *Constr. Build. Mater.* 2021; 305: 124819. [doi:10.1016/j.conbuildmat.2021.124819](https://doi.org/10.1016/j.conbuildmat.2021.124819)
 29. Huang X, Liu G, Zheng Y, Luo H. The performance of magnesium phosphate cement in negative temperature environment: A state-of-the-art review. *J. Build. Eng.* 2023; 76: 107278. [doi:10.1016/j.jobe.2023.107278](https://doi.org/10.1016/j.jobe.2023.107278)
 30. Xin Y., Sun W., Hu X., Wang X., Hou D., Xv F., Gao Y., Shen P., Chen X., Min Q. The effect of borax-urea composite retarder on the hydration process, microstructure and properties of magnesium phosphate cement. *Constr. Build. Mater.* 2025; 493: 143108. [doi:10.1016/j.conbuildmat.2025.143108](https://doi.org/10.1016/j.conbuildmat.2025.143108)
 31. Tao R., Lv T., Zhang J., Li Z., Hou D. Synergistic enhancement of magnesium phosphate cement by fly ash and dredged sludge: Hydration behavior and performance. *Constr. Build. Mater.* 2025; 495: 143709. [doi:10.1016/j.conbuildmat.2025.143709](https://doi.org/10.1016/j.conbuildmat.2025.143709)
 32. Wang N., Li Y., Long S., Lin H., Wang Z., Liu X. Research on the preparation and pore structure of porous brucite-based magnesium phosphate cement. *Constr. Build. Mater.* 2025; 478: 141416. [doi:10.1016/j.conbuildmat.2025.141416](https://doi.org/10.1016/j.conbuildmat.2025.141416)
 33. Van der Merwe EM, Strydom CA, Potgieter JH. Hydration of medium reactive magnesium oxide using hydration agents. *J Therm Anal Calorim.* 2006; 84(2):467-471. [doi:10.1007/s10973-005-7291-6](https://doi.org/10.1007/s10973-005-7291-6)

34. Ma H, Gong W, Yu H, Sun W. The effect of different hydration media on magnesia. *Discov Mater.* 2021;1:17. [doi:10.1007/s43939-021-00017-9](https://doi.org/10.1007/s43939-021-00017-9)
35. Xu B., Winnefeld F., Kaufmann J., Lothenbach B. Influence of magnesium-to-phosphate ratio and water-to-cement ratio on hydration and properties of magnesium potassium phosphate cements. *Cem. Concr. Res.* 2019; 123: 105781. [doi:10.1016/j.cemconres.2019.105781](https://doi.org/10.1016/j.cemconres.2019.105781).
36. Qin J, Qian J, Dai X, You C, Ma H, Li Z. Effect of water content on microstructure and properties of magnesium potassium phosphate cement pastes with different magnesia-to-phosphate ratios. *J. Am. Ceram. Soc.* 2021; 104 (6): 2799-2819. [doi:10.1111/jace.17695](https://doi.org/10.1111/jace.17695).
37. Dong J, Zheng W, Chang C, Wen J, Xiao X. Function and effect of borax on magnesium phosphate cement prepared by magnesium slag after salt lake lithium extraction. *Constr. Build. Mater.* 2023; 366: 130280. [doi:10.1016/j.conbuildmat.2022.130280](https://doi.org/10.1016/j.conbuildmat.2022.130280)
38. Gelli R, Tonelli M, Martini F, Calucci L, Borsacchi S, Ridi F. Effect of borax on the hydration and setting of magnesium phosphate cements. *Constr. Build. Mater.* 2022; 348: 128686. [doi:10.1016/j.conbuildmat.2022.128686](https://doi.org/10.1016/j.conbuildmat.2022.128686)
39. Garcia-Lodeiro I, Chhaiba S, Husillos-Rodriguez N, Palomo Á, Kinoshita H. Development of Magnesium Phosphate Cement Based on Low-Grade MgO. *Materials.* 2025; 18 (6): 1198. [doi:10.3390/ma18061198](https://doi.org/10.3390/ma18061198)
40. Le Rouzic M, Chaussadent T, Stefan L, Saillio M. On the influence of Mg/P ratio on the properties and durability of magnesium potassium phosphate cement pastes. *Cem. Concr. Res.* 2017; 96: 27 - 41. [doi:10.1016/j.cemconres.2017.02.033](https://doi.org/10.1016/j.cemconres.2017.02.033)
41. Wang C, Chen B, Wang Y, Vo TL, Rezania M, He F. Influencing Mechanism of Magnesium-to-Phosphate Ratio on the Rheology and Microstructure Development of 3D-Printed Magnesium Phosphate Cement at Early Hydration. *J. Mater. Civ. Eng.* 2025; 37 (11): 04025385. [doi:10.1061/JMCEE7.MTENG-19889](https://doi.org/10.1061/JMCEE7.MTENG-19889)
42. Zhao Y, Lothenbach B, Hu Z, Xu B. Optimizing Mg/PO₄ molar ratio for ultra-high-performance steel fiber-reinforced magnesium potassium phosphate cement-based composite. *Cem. Concr. Res.* 2026; 201: 108126. [doi:10.1016/j.cemconres.2025.108126](https://doi.org/10.1016/j.cemconres.2025.108126)
43. Zhang M, Pei Y, Zhang Q, Qian J. Effect of M/P ratio, w/c ratio, and additive contents on rheological properties of seawater mixed magnesium phosphate cement system. *Constr. Build. Mater.* 2024; 424: 135859. [doi:10.1016/j.conbuildmat.2024.135859](https://doi.org/10.1016/j.conbuildmat.2024.135859)
44. Feng H, Lu S, Guo A, Yu Z. Research progress on the water resistance of magnesium phosphate cement-based composites. *J. Mater. Sci.* 2025; 60 (38): 17326 - 17346. [doi:10.1007/s10853-025-11462-9](https://doi.org/10.1007/s10853-025-11462-9)
45. Xie W., Chen B., Rong H., Li J. Unveiling the impact of water-to-binder ratio on foaming behavior of foamed magnesium phosphate cement. *Constr. Build. Mater.* 2025; 474: 141072. [doi:10.1016/j.conbuildmat.2025.141072](https://doi.org/10.1016/j.conbuildmat.2025.141072).
46. Zheng W., Dong J., Wen J., Chang C., Xiao X. Effects of water-to-cement ratios on the properties of magnesium potassium phosphate cement prepared with lithium-extracted magnesium residue. *Appl. Sci.* 2021; 11 (9): 4193. [doi:10.3390/app11094193](https://doi.org/10.3390/app11094193).
47. Wang X, Hu X, Chong L, Yang J, Shi C. Effects of the combination of NH₄H₂PO₄ and KH₂PO₄ on the interfacial bond between magnesium phosphate cement and steel fiber. *Constr. Build. Mater.* 2023; 407: 133405. [doi:10.1016/j.conbuildmat.2023.133405](https://doi.org/10.1016/j.conbuildmat.2023.133405)
48. Li L, Yu H, Dong J, Ma H, Yu W, Fang K, Wu C, Wen J, Li W. Optimal selection of magnesium phosphate cement systems for lunar soil concrete: Potassium, ammonium, calcium, and sodium magnesium phosphate cements. *Adv. Space Res.* 2025; 75 (6): 5205 - 5226. [doi:10.1016/j.asr.2024.12.059](https://doi.org/10.1016/j.asr.2024.12.059)
49. Fan S, Chen B. Experimental study of phosphate salts influencing properties of magnesium phosphate cement. *Constr. Build. Mater.* 2014; 65: 480 - 486. [doi:10.1016/j.conbuildmat.2014.05.021](https://doi.org/10.1016/j.conbuildmat.2014.05.021)
50. Yuan J, Huang X, Chen X, Ge Q, Zhang Z. Early-age mechanical properties and hydration degrees of magnesium phosphate cement paste in freezing winter of cold regions. *Constr. Build. Mater.* 2022; 345: 128337. [doi:10.1016/j.conbuildmat.2022.128337](https://doi.org/10.1016/j.conbuildmat.2022.128337)
51. Yuan J, Huang X, Chen X, Zhang Z, Ge Q, Liu Y. Potentialities of magnesium phosphate cement-based ultra-high-performance concrete in extremely cold weather construction. *Constr. Build. Mater.* 2024; 456: 139297. [doi:10.1016/j.conbuildmat.2024.139297](https://doi.org/10.1016/j.conbuildmat.2024.139297)
52. Li Y, Ma G, Wang Z. Experimental study on brucite-based magnesium phosphate cement in cold environment. *Constr. Build. Mater.* 2025; 142221. [doi:10.1016/j.conbuildmat.2025.142221](https://doi.org/10.1016/j.conbuildmat.2025.142221)
53. Jia X, Li J, Wang P, Qian J, Tang M. Preparation and mechanical properties of magnesium phosphate cement for rapid construction repair in ice and snow. *Constr. Build. Mater.* 2019; 229: 116927. [doi:10.1016/j.conbuildmat.2019.116927](https://doi.org/10.1016/j.conbuildmat.2019.116927)
54. Luo X., Lai Z., Liu Z., Xiao R., Chen J., Lu Z., Lv S., Wang J. Effect of Modified Magnesium Oxide on the Properties of Magnesium Phosphate Cement under a Negative Temperature Environment. *Materials.* 2022; 15 (24): 9047. [doi:10.3390/ma15249047](https://doi.org/10.3390/ma15249047)
55. Wang Q., Huang X., Xu S., Wang F. Mechanical performance and hydration characteristics of modified magnesium phosphate cement concrete under negative temperatures. *Constr. Build. Mater.* 2025; 493: 143186. [doi:10.1016/j.conbuildmat.2025.143186](https://doi.org/10.1016/j.conbuildmat.2025.143186).
56. Liu Z, Lai Z, Luo X, Xiao R, Chen J, Lu Z. Properties of magnesium phosphate cement reinforced with natural brucite fiber. *Constr. Build. Mater.* 2023; 393: 132057. [doi:10.1016/j.conbuildmat.2023.132057](https://doi.org/10.1016/j.conbuildmat.2023.132057)
57. Qoku E, Scheibel M, Bier T, Gerz A. Phase development of different magnesium phosphate cements at room temperature and elevated temperatures. *Constr. Build. Mater.* 2021; 272: 121654. [doi:10.1016/j.conbuildmat.2020.121654](https://doi.org/10.1016/j.conbuildmat.2020.121654)
58. Kasprzhitskii A, Lazorenko G, Khater A, Yavna V. Mid-infrared spectroscopic assessment of plasticity characteristics of clay soils. *Minerals.* 2018; 8 (5): 184. [doi:10.3390/min8050184](https://doi.org/10.3390/min8050184)
59. Yavna VA, Kasprzhitskii AS, Lazorenko GI, Kochur AG. Study of IR spectra of a polyminerall natural association of phyllosilicate minerals. *Opt. Spectrosc.* 2015; 118 (4): 529 - 536. [doi:10.1134/S0030400X15040220](https://doi.org/10.1134/S0030400X15040220)
60. Kasprzhitskii A, Lazorenko G, Yavna V, Daniel P. DFT theoretical and FT-IR spectroscopic investigations of the plasticity of clay minerals dispersions. *J. Mol. Struct.* 2016; 1109: 97 - 105. [doi:10.1016/j.molstruc.2015.12.064](https://doi.org/10.1016/j.molstruc.2015.12.064)
61. Cui Y, Wang Y, Li H, Yang Q. A study on particle size of slag on properties of magnesium potassium phosphate cement. *Int. J. Appl. Ceram. Technol.* 2024; 21 (5): 3220 - 3228. [doi:10.1111/ijac.14768](https://doi.org/10.1111/ijac.14768)
62. Kasprzhitskii AS, Lazorenko GI, Sulavko SN, Yavna VA, Kochur AG. A study of the structural and spectral characteristics of free and bound water in kaolinite. *Opt. Spectrosc.* 2016; 121 (3): 357 - 363. [doi:10.1134/S0030400X16090113](https://doi.org/10.1134/S0030400X16090113)
63. Nazdracheva TF, Kukharskii AV, Kasprzhitskii AS, Lazorenko GI, Yavna VA, Kochur AG. Study of the Features of the Formation of Water Films on the Surfaces of Montmorillonite and Kaolinite by Infrared Spectroscopy. *Opt. Spectrosc.* 2021; 129 (2): 270 - 275. [doi:10.1134/S0030400X21020107](https://doi.org/10.1134/S0030400X21020107)
64. Li Y, Long S, Wang N, Lin H, Wang Z. Toward sustainable magnesium phosphate cement: Deciphering the dissolution and reaction mechanisms of magnesium hydroxide in acid phosphate systems. *Compos. Part B Eng.* 2025; 302: 112542. [doi:10.1016/j.compositesb.2025.112542](https://doi.org/10.1016/j.compositesb.2025.112542)
65. Yang Y, Han J, Liu R. Understanding hydration properties of magnesium potassium phosphate cement with low magnesium-to-phosphate ratio. *Constr. Build. Mater.* 2024; 416: 135221. [doi:10.1016/j.conbuildmat.2024.135221](https://doi.org/10.1016/j.conbuildmat.2024.135221)
66. Goldberg MA, Krohicheva PA, Fomin AS, Khairutdinova DR, Antonova OS, Baikin AS, Smirnov VV, Fomina AA, Leonov AV,

Mikheev IV, Sergeeva NS, Akhmedova SA, Barinov SM, Komlev VS. Insitu magnesium calcium phosphate cements formation: From one pot powders precursors synthesis to in vitro investigations. *Bioact. Mater.* 2020; 5 (3): 644 - 658.
[doi:10.1016/j.bioactmat.2020.03.011](https://doi.org/10.1016/j.bioactmat.2020.03.011)